Article

Fast-Processing DEM-Based Urban and Rural Inundation Scenarios from Point-Source Flood Volumes

Kay Khaing Kyaw [1,*] , Federica Bonaiuti [1,2], Huimin Wang [1], Stefano Bagli [3], Paolo Mazzoli [3], Pier Paolo Alberoni [4] , Simone Persiano [1,5] and Attilio Castellarin [1]

[1] Department of Civil, Chemical, Environmental and Materials Engineering (DICAM), University of Bologna, 40136 Bologna, Italy; federica.bonaiuti@adbpo.it (F.B.); huimin.wang@studio.unibo.it (H.W.); simone.persiano@unipolsai.it (S.P.); attilio.castellarin@unibo.it (A.C.)

[2] Autorità di Bacino Distrettuale del Fiume Po, Strada Garibaldi 75, 43121 Parma, Italy

[3] GECOsistema Srl, 47923 Rimini, Italy; stefano.bagli@gecosistema.com (S.B.); paolo.mazzoli@gecosistema.com (P.M.)

[4] Arpae-SIMC, Hydro-Meteo-Climate Service of the Regional Agency for Prevention, Environment and Energy (ARPAE), 40122 Bologna, Italy; palberoni@arpae.it

[5] Catastrophe Risk Modeling & Mitigation, UnipolSai Assicurazioni S.p.A., Piazza della Costituzione 2/2, 40128 Bologna, Italy

* Correspondence: kaykhaing.kyaw2@unibo.it

Abstract: Flooding has always been a huge threat to human society. Global climate change coupled with unsustainable regional planning and urban development may cause more frequent inundations and, consequently, higher societal and economic losses. In order to characterize floods and reduce flood risk, flood simulation tools have been developed and widely applied. Hydrodynamic models for inundation simulation are generally sophisticated, yet they normally require massive setup and computational costs. In contrast, simplified conceptual models may be more easily applied and efficient. Based on the Hierarchical Filling-and-Spilling or Puddle-to-Puddle Dynamic Filling-and-Spilling Algorithms (i.e., HFSAs), Safer_RAIN has been developed as a fast-processing DEM-based model for modelling pluvial flooding over large areas. This study assesses Safer_RAIN applicability outside the context for which it was originally developed by looking at two different inundation problems with point-source flooding volumes: (1) rural inundation modelling associated with levee breaching/overtopping; (2) urban flooding caused by drainage systems outflow volumes.

Keywords: DEM-based model; hydrodynamic models; point-source flooding volumes; rural inundation modelling; Safer_RAIN; urban flooding

1. Introduction

Flooding has significant effects on citizens and economic activities in Europe, with river and coastal flooding affecting millions of people. There has been a rise in the yearly flooded area and the number of people impacted, although there has been a significant decline in flood-related deaths [1]. Climate change and anthropogenic pressure are contributing to an increase in both the frequency and intensity of severe flood events. High-resolution flood monitoring is essential throughout the disaster management process, starting with the early warning phase and extending to the emergency and civil protection stage, damages evaluation, indemnification, and loss control [2]. In addition, the change in land use due to urbanisation, particularly the transformation of forested or agricultural fields into impermeable metropolitan areas, often has a significant influence on climate-related problems at the regional level. This may result in heightened vulnerability to river floods, among other consequences [3,4]. Therefore, it is crucial that flood risk management plans take into account the unique characteristics of the regions they represent and devise specific solutions in alignment with the particular requirements and precedence of those places. These plans should promote efficient cooperation across river basin districts and facilitate

the achievement of environmental objectives set by community law at the same time. In order to have a reliable and useful tool for making informed decisions about flood risk management, it is imperative to create flood hazard maps and flood risk maps that include data on potential sources of environmental contamination caused by flooding [5].

Flood modelling offers valuable data to facilitate flood risk evaluation and mitigation. The accuracy of flood simulation results is strongly dependent on the quality of essential input data related to topography and hydrometeorology. This includes data such as elevation, land use/land cover maps, soil properties, rainfall estimates, river geometry, initial and boundary conditions, as well as infrastructure details. Among these inputs, the digital elevation model (DEM) stands out as a critical component, as it plays a fundamental role in determining the flow paths and drainage patterns across the landscape. Presently, there is a greater availability of high-resolution DEMs which have been integrated into urban flood models and vulnerability assessments [6–8]. Despite this, it is generally accepted that the quality of the topographic data or DEM has a substantial effect on the validity of hydrodynamic modelling results [9–11]. Due to recent progress in computer power and the accessibility of high-quality data, hydrodynamic models are now capable of conducting precise flood forecasts at high resolutions. These models can provide detailed information on the timing and location of flood inundation, even in intricate urban settings [12,13]. The primary objective of flood modelling is to accurately determine the amount of flood inundation. This is achieved by combining streamflow prediction models with hydrodynamic models that have been well calibrated [14–16]. In recent decades, the availability of Geographic Information System (GIS) tools and data, such as DEMs, has presented a unique opportunity for the development of low-complexity DEM-based methods for floodplain delineation, replacing hydrodynamic models in some cases [17–20]. Among these DEM-based methods, those using a morphologic algorithm to distinguish between flooded and non-flooded areas demonstrate better efficiency and need less computing power [21–25].

SaferPlaces is a flood inundation simulation platform that utilises advanced techniques in climate, hydrological, hydraulic, topographic, and economic modelling to evaluate the hazard and risk of pluvial, fluvial, and coastal flooding in urban areas, both at present and in the future (see https://saferplaces.co/ (accessed on 15 January 2024) and documentation therein for additional details). The purpose of this platform is to simplify the process of identifying and evaluating measures and plans to reduce the danger of flooding. It also provides information to support strategies for adapting to climate change and reducing the risk of disasters. Additionally, it enables different stakeholders to reach agreements and collaborate on building resilience. SaferPlaces is a continuation of the successful 2017 Climate KIC Pathfinder project "PLACES—Pluvial flood hazard and risk assessment and mitigation in European cities". The primary objective is to improve, develop, test, and demonstrate the effectiveness and scalability of a flood hazard and risk mapping and assessment service in an urban setting. This service is vital for the development of climate adaptation strategies and disaster risk reduction initiatives. Furthermore, it aims to promote discussions among various stakeholders and to identify measures and strategies for reducing disaster risks and adapting to climate change. It also intends to explore potential business opportunities and economic benefits for making behavioural and land-use changes. This will be achieved by implementing nature-based or ecosystem-based solutions, such as natural water retention and urban requalification. Detailed hydrologic–hydraulic numerical modelling is resource intensive and, as a result, inadequate for performing consistent hazard assessments throughout large urban settlements. Many studies have highlighted the potential of fast-processing DEM-based methods, such as the Hierarchical Filling-and-Spilling or Puddle-to-Puddle Dynamic Filling-and-Spilling Algorithms (abbreviated herein as HFSAs), considering the steadily increasing availability of LiDAR high-resolution DEMs (Digital Elevation Models). Safer_RAIN is a module of SaferPlaces that uses a fast-processing HFSA to accurately map pluvial flooding in large metropolitan areas. This is achieved by considering the spatial distribution of rainfall input and infiltration processes using a

pixel-based Green-Ampt model. The modelling approach and algorithms of Safer_RAIN have been originally presented in [26] and are not reported here for the sake of conciseness. The methodology focuses on utilising raster manipulation techniques and hydrological GIS tools for DEM analysis. An interested reader can refer to [26] for additional details and a presentation of the validation of the approach against real-world pluvial inundation events.

Safer_RAIN was originally designed to simulate urban flooding caused by spatially uniform precipitation, and in the present study, we aim to investigate its possibilities beyond its original intended use. We present two applications of Safer_RAIN for producing urban and rural flooding scenarios associated with breaches in small stream levee-systems, and drainage system outflow volumes. By expanding the scope of Safer_RAIN, we want to demonstrate its versatility and effectiveness in simulating various flood scenarios.

Firstly, conventional flood risk management mostly depends on structural measures to reduce the impact of floods, rather than using comprehensive strategies like expanding river capacity and restricting development in flood-prone areas [27]. Practically, the implementation of structural solutions such as levees, dams, and built channels promotes the growth of urban and agricultural areas on floodplains, as it instills the belief among the public that the danger of flooding has been diminished [28]. Additionally, there are rural communities that have been affected by floods resulting from levee breaches [29]. This highlights the increasing demand for simulating rural flooding resulting from possible levee failures in order to better understand and address the challenges faced by these areas and the residual risk of flooding. Therefore, we conducted benchmarking activities to test Safer_RAIN's ability to simulate rural flood inundation, using the outputs of HEC-RAS two-dimensional hydrodynamic modelling.

Secondly, recent studies have shown that drainage conditions can have a significant impact on urban rainfall-runoff processes [30–32]. Alongside land use, the urban drainage network system is considered a major contributor to urban inundations [33,34]. Previous research indicates that a poorly designed or inadequate drainage system can lead to flooding in urban areas, primarily due to outflow volumes [35–37]. Motivated by these findings, we utilise Safer_RAIN to simulate flooding in urban areas caused by the limited capacity of the drainage system. To assess the accuracy of our simulations, we compare the results with those obtained from Hydro AS 2D hydrodynamic modelling, using identical boundary conditions in Safer_RAIN.

The results of these two different applications enable us to better understand the true potential and versatility of Safer_RAIN for modelling and mapping flood hazards in rural and urban areas.

This paper is organized in the following way: Section 2—Materials and Methods; Section 3—Application of Safer_RAIN for generating inundations scenarios from point-source flood volumes; Section 4—Results; Section 5—Discussion; and Section 6—Conclusions.

2. Materials and Methods

2.1. DEM-Based Hierarchical Filling-and-Spilling Algorithm "Safer_RAIN"

Hydrodynamic models typically require extensive setup and computational resources, making them impractical for quickly responding to emergent flooding events or accurately characterizing flood hazards across large geographical areas with high horizontal resolutions (e.g., 1 m) [38]. As a result, there is a need for reliable models that can rapidly simulate large areas at high horizontal resolutions in inundation modelling. To overcome the limitations and drawbacks of hydrodynamic inundation models, simplified conceptual models have been developed. These simplified models offer significantly shorter runtime compared to hydrodynamic models. The SaferPLACES project has successfully developed and implemented simplified DEM-based flood hazard modelling modules that address the three primary sources of flooding: Safer_RIVER for fluvial flooding, Safer_COAST for coastal flooding, and Safer_RAIN for pluvial flooding [26]. In this article, our focus is on Safer_RAIN as we apply this module to address a specific inundation problem faced by the

drainage plain of the Pisciatello stream in the province of Forlì-Cesena, Northern Italy, as well as certain areas in Milan, Italy.

The availability of high-resolution LiDAR DEMs, which can accurately capture and represent surface depressions in the landscape [39], has led to the widespread use of raster or DEM-based processing methods for quickly mapping flooding hotspots across large areas. One popular approach is the hierarchical Filling-and-Spilling (HFS) algorithm family, which has been implemented and improved within the Safer_RAIN module [40–42]. These algorithms utilise LiDAR DEMs to efficiently identify and analyse flooding patterns, allowing for rapid and accurate mapping of flood-prone areas.

The classical implementation of HFS algorithms typically incorporates several simplifying assumptions. Firstly, the drainage direction is determined using the traditional D8 method [43]. The dynamic nature of the flooding process is disregarded as these algorithms do not solve hydrodynamic equations. Instead, they apply mass balance equations to the hierarchical system of vertical and horizontal depressions, which are identified and delineated from high-resolution DEMs. When a depression reaches its maximum filling level, any excess water volume is distributed to downstream depressions based on their storage capacity. Additionally, the HFS algorithms assume that the surface is impermeable, and that rainfall is uniformly distributed across the area. These two hypotheses are applicable specifically to traditional applications of HFS algorithms.

The application of Safer_RAIN primarily involves two phases: (i) DEM pre-processing, which is similar to other previously proposed HFS algorithms, and (ii) an original depression-flooding phase. During intense precipitation events that affect cities, surface depressions and microtopography in the study area play a crucial role in water retention. The DEM pre-processing is designed to identify depressions based on a high-resolution input DEM. Along with depression extraction, the hierarchical structure of the depressions is established using a top-down level-set method (see Figure 1 for reference) [41]. The connections between upstream and downstream depressions at different locations and elevations are modelled under the simplifying assumption of the D8 method. In the second phase, Safer_RAIN simulates inundation using a level-set method that allows for partial flooding of the depression system, relaxing the last two assumptions mentioned above. Infiltration losses are represented through a pixel-based adaptation of the event-based Green-Ampt infiltration model [44], and the rainfall input can be non-uniform in space, described by a raster map. This phase requires information about the rainstorm event to be simulated, which can be either synthetic or real, such as a weather radar map showing the accumulated rainfall depth in a given time interval. For a detailed description of the Safer_RAIN algorithm, its validation, and applications to different case studies, readers are referred to [26].

It is important to note that Safer_RAIN focuses on representing the hydrostatic and final extent of inundation, rather than the dynamics of flooding. As a result, the inundations simulated by Safer_RAIN are expected to provide a more accurate representation of water depth at the end of the rainstorm event, while potentially underestimating the local maximum water depth during the event itself. However, as stated in [26], the runtime of the flooding phase is remarkably short, even for large computational domains. This makes the algorithm well suited for simulating numerous flooding scenarios, which is essential for inundation forecasting/nowcasting or stochastic characterization of flood hazards (e.g., [45]).

2.2. Metrics and Diagrams for Assessing the Reliability of Safer_RAIN Results

In order to assess the performance of Safer_RAIN, we conduct benchmarking exercises by comparing its output to that of a numerical 2D hydrodynamic model. Additionally, we compare different flooding scenarios generated by Safer_RAIN, taking into account simulated flood maps, the FAI index, and the spatial frequency of pixel-based simulated water depths. We also analyse differences between simulated water depths for pairs of inundation scenarios. Throughout the results subsections of Sections 3 and 4, we present these metrics and indices using tables and diagrams to provide a comprehensive evaluation.
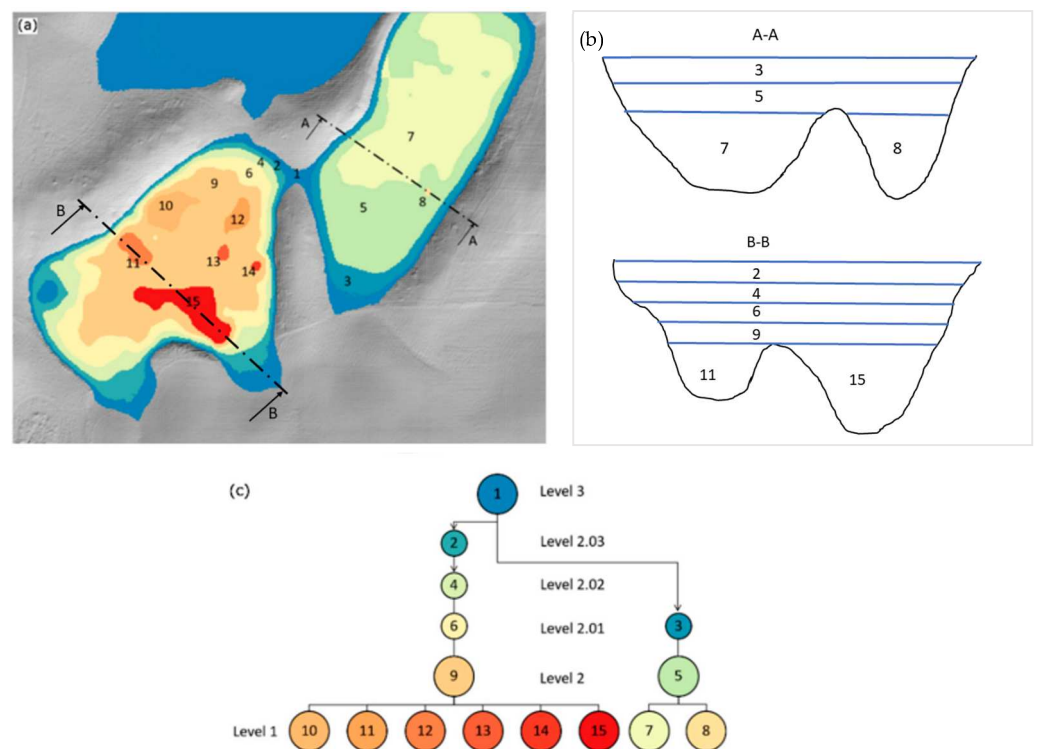
Figure 1. Nested depressions structure: (**a**) plan view; (**b**) cross-sectional views; and (**c**) hierarchical tree, representing the intermediate-level depressions with specific colours and the corresponding filling level for the bottom-up flooding phase indicated with numbers [26].

2.2.1. Flood Maps

The flood maps present a qualitative representation of the extent of inundation and water depth across the study area. However, due to the inherent uncertainty of Safer_RAIN, only pixels with a water depth exceeding 0.1 m are considered to be flooded. This approach takes into account the uncertainty associated with the simulation results and ensures a conservative assessment of the flooded areas.

2.2.2. FAI Index

The Flood Area Index is employed to compare the extent of flooded areas between pairs of inundation scenarios. This index allows for a quantitative assessment of the differences in the flooded area between these scenarios, providing valuable insights into the variations in flood extent. The FAI is defined as:

$$\text{FAI} = \frac{A}{A + B + C} \tag{1}$$

where:

A is the areas that are identified as flooded in both simulations;
B is the area that is flooded in one of the two simulations only;
C is the area that is flooded in the other simulation only.
FAI values range from 0 to 1. The closer the FAI value is to 1, the higher the similarity between the inundation extents in the two simulations.

2.2.3. Distribution of Water Depths

In addition to comparing the extent of inundated areas using flood maps and the Flood Area Index (FAI), we also conduct a quantitative assessment of the simulated water depth. This involves analysing the cumulative frequency, or more precisely, the exceedance probability of pixel-based simulated water depths across the computational domain. Fur-

thermore, we compare pairs of simulated inundation scenarios by plotting the exceedance probability of differences between local values (pixels) of simulated water depths. In the latter case, a difference of 0 indicates that the water depths simulated for both scenarios are identical or that the pixel remains dry (non-flooded) in both simulated scenarios. The larger the area with a water-depth difference of 0, the more similar the two simulation results. Additionally, smaller differences between water depths indicate closer simulation results.

3. Application of Safer_RAIN for Generating Inundation Scenarios from Point-Source Flood Volumes

3.1. Rural Inundations from Minor Streams: Study Area, Available Data, and Analyses

The study area is situated in the drainage plain of the Pisciatello stream, in the province of Forlì-Cesena, Northern Italy. This triangular-shaped area covers a total of 1352 hectares, as shown in Figure 2. It is located within the municipality of Cesenatico, and it is positioned near the Adriatic Sea. The Pisciatello stream runs along the southern border of the study area, while the northern border aligns with the embankment of state road SS304. The municipality of Cesenatico is seeking cost-effective tools for conducting high-resolution flood hazard modelling and mapping to develop a more secure and sustainable urban planning strategy. This objective serves as the original motivation for testing the capabilities of Safer_RAIN in this context. We evaluate the performance of Safer_RAIN relative to the 2D hydrodynamic model available within the HEC-RAS modelling environment [46].
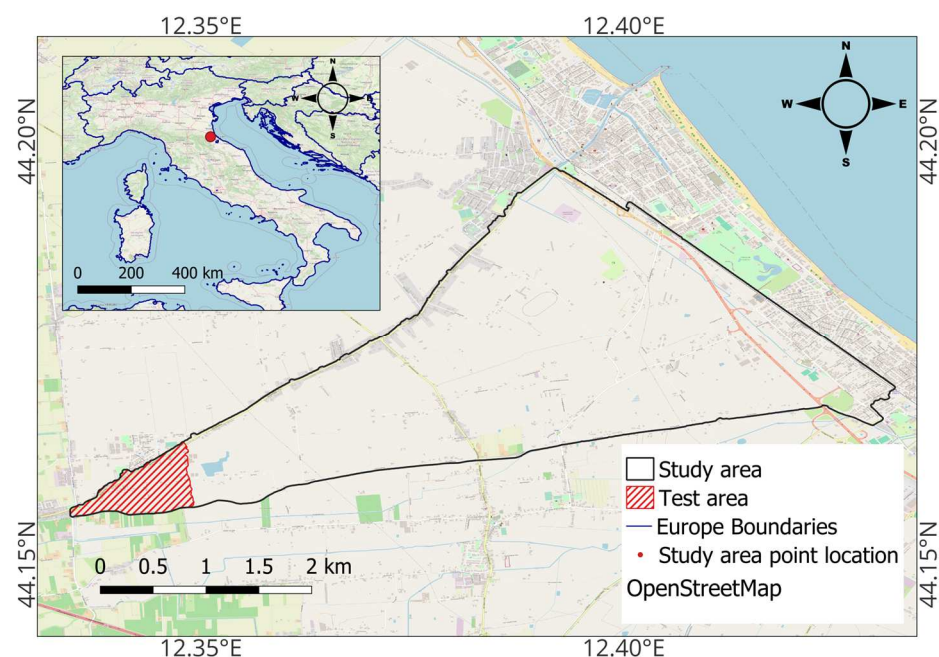

Figure 2. Overall study area (Northern Italy) and test area: small portion of the region of interest used for testing HEC-RAS implementations with different resolutions.

Terrain data is described by a 1 m resolution LiDAR DEM in both Safer_RAIN and HEC-RAS. The DEM is obtained from the Italian Ministry of the Environment's National Geoportal (http://www.pcn.minambiente.it/mattm/en/ (accessed on 15 January 2024)). Given the very different natures of the two models, specific modelling strategies and choices need to be adopted in order for the results to be comparable. Two aspects are of particular importance: the representation of buildings and the representation of the inflow flood volumes needed for modelling the inundation of the floodplain.

The presence of buildings can be accurately modelled in Safer_RAIN by incorporating them into the digital surface model used in the computational domain [26]. Different modelling strategies have been adopted in the literature to represent urban environments within 2D hydrodynamic inundation models, with variations aimed at controlling computational

costs while sacrificing modelling accuracy [47]. In this study, we considered two modelling strategies for implementing the 2D hydrodynamic model. The first strategy explicitly accounts for the presence of buildings by elevating the building footprint above the ground within the computational mesh. We refer to this strategy as "DEM with extruded buildings" in the text. In this modelling approach, Manning's roughness coefficient remains constant across the entire study area. The second strategy, referred to as "DEM without buildings," does not include the representation of buildings within the computational domain. Instead, it assigns a very high Manning's roughness coefficient to the developed areas to account for their higher resistance to inundation propagation.

Regarding the inflow flood volumes, Safer_RAIN only requires a flood volume as input at a specific location within the computational mesh. However, for HEC-RAS 2D inundation simulations, a complete inflow hydrograph is necessary. In this study, we utilise three different hydrographs to simulate various breaching evolutions and observe their impact on the inundation dynamics and the similarities between Safer_RAIN and HEC-RAS simulations (Figure 3a). All three hydrographs are associated with a flood volume corresponding to a 200-year return period, based on the most recent studies available for the study area [48]. In Figure 3a, hydrograph (a) represents a scenario where the breaching phenomenon occurs rapidly, with the complete formation of the levee breach taking place within 1.5 h. The maximum outflow discharge for this scenario is 67.4 m^3/s. Hydrographs (b) and (c), on the other hand, depict slower formations of the breaches and are characterized by maximum discharges of 10 m^3/s and 5 m^3/s, respectively.


(**a**)   (**b**)
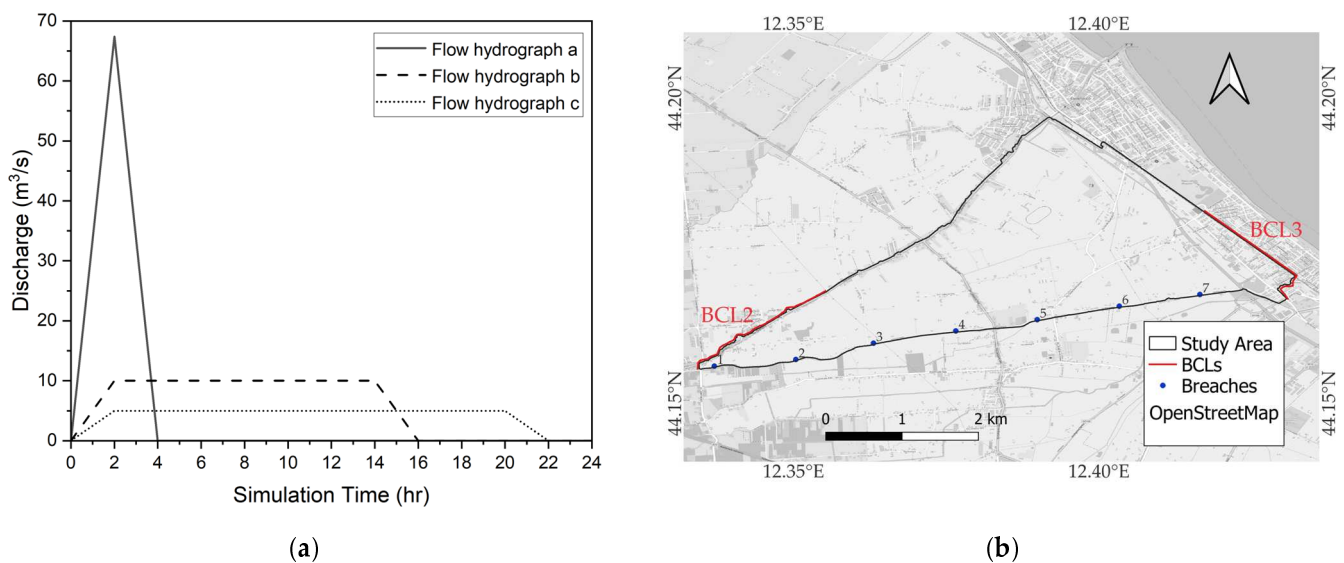
Figure 3. (**a**) Inflow hydrographs used for simulating breaches with HEC-RAS. (**b**) The overall study area indicating location of synthetic breaches and outlet boundary condition lines (BCLs).

3.2. Urban Inundations from Drainage System Outflows: Study Area, Available Data, and Analyses

In this study, we are testing the capabilities of Safer_RAIN to simulate flooding caused by the outflow volumes from drainage system manholes during heavy rainfall events. Typically, Safer_RAIN is used to simulate urban pluvial flooding without considering the presence and effects of urban drainage systems. However, we aim to expand its application and assess its ability to accurately simulate this specific type of flooding. Our focus is on a sensitive area in the northeastern district of Milan, known for its susceptibility to pluvial flooding. To ensure the accuracy of our simulations, we have collaborated closely with Metropolitana Milanese Spa (MM Spa), the organization responsible for managing Milan's drainage system. MM Spa has provided us with their numerical hydrodynamic model of the drainage system, which we have used to identify the locations and volumes of the outflowing manholes during critical storms in our study district. The storms in our study

typically last around 90 min, so we have chosen to analyse a storm duration of 90 min. We have considered three different scenarios with return periods of 20, 50, and 100 years to capture a range of rainfall intensities. Using the volumes obtained from MM Spa's model as local water volume sources, we have incorporated them into Safer_RAIN to simulate the inundated areas. In Safer_RAIN, we utilise a LiDAR Digital Elevation Model (DEM) with a resolution of 1 m for our analysis. To accurately represent the depressions in the terrain, we set a discretization interval of 0.05 m and established a threshold volume of 300 m^3. In Figure 4, we have also included the locations of the outflowing manholes, as identified through the numerical simulations conducted with MM Spa's model.Additionally, we incorporate the extrusion of buildings into our analysis using OpenStreetMap. The results of our simulations are depicted in Figure 5, which illustrates the flooded areas.

(a)   (b)   (c)
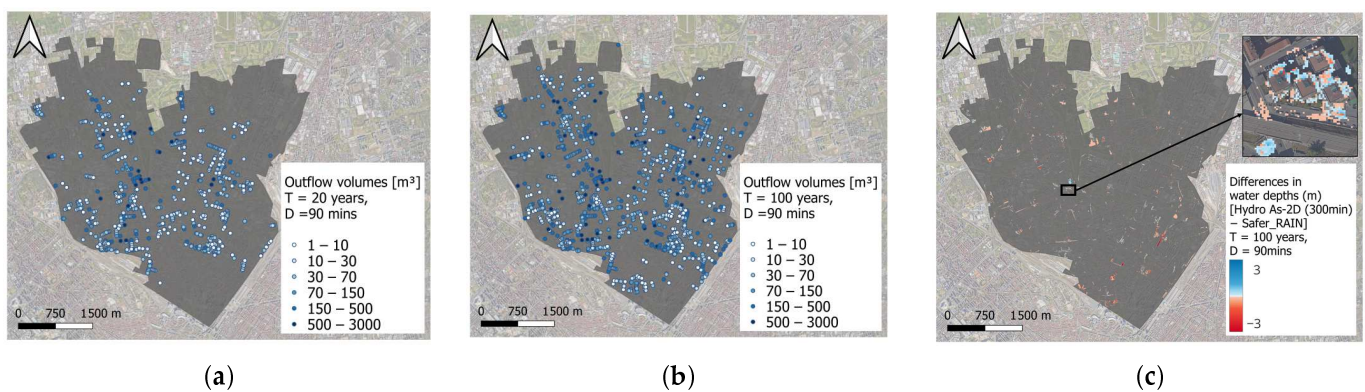
Figure 4. (**a**) Outflow volumes from drainage system as modelled by MM Spa for 90 min rainfall events associated with 20 years return period. (**b**) Outflow volumes from drainage system as modelled by MM Spa for 90 min rainfall events associated with 100 years return period. (**c**) Differences between water depths simulated by Hydro_AS-2D (after 300 min) and Safer_RAIN for 100-year return period.
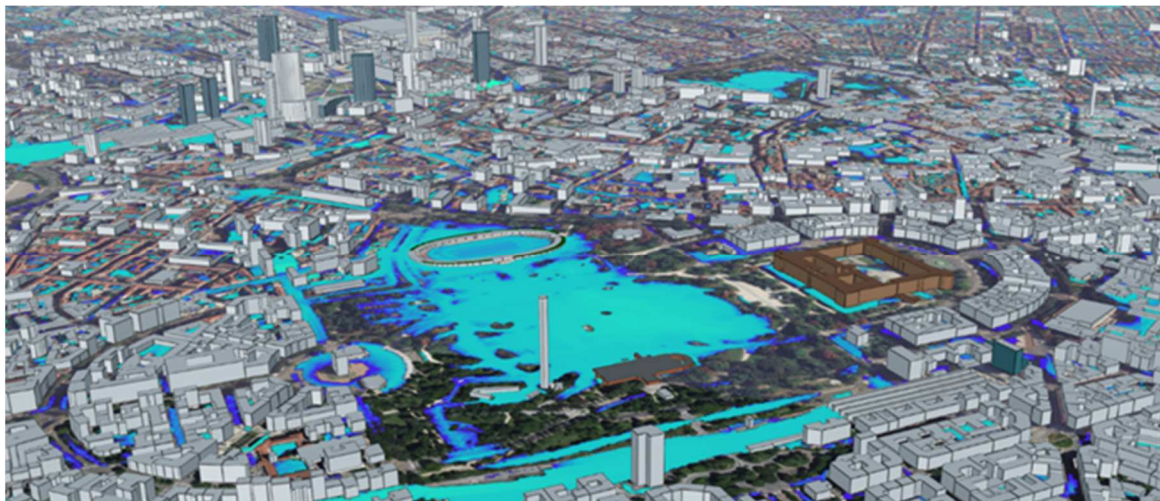
Figure 5. 3D rendering of inundated areas simulated by Safer_RAIN (Milan, Italy).

To ensure the accuracy and reliability of Safer_RAIN in simulating pluvial flooding, we compare its output with the results obtained from a benchmark hydrodynamic model known as Hydro_AS-2D. Hydro_AS-2D is an advanced hydrodynamic model that has been developed by IBH (Water, Environment and Infrastructure, Austria). It is a state-of-the-art model that operates in two dimensions (2D). The Hydro_AS-2D model is capable of solving shallow water equations. Additionally, it provides users with the option to compute pluvial floods and include the rainfall-runoff model in the simulation process. It is widely recognized for its capabilities in accurately representing complex hydrodynamic processes

associated with urban flooding. For our comparative analysis, we adopt the same boundary conditions that were applied in the Safer_RAIN simulations. This includes utilising the outflow volumes obtained from the three rainfall scenarios considered in our study.

We consider every manhole as a point source of water, assigning each one to the nearest node in the computational meshes of Safer_RAIN and Hydro_AS-2D. In the case of Hydro_AS-2D, we use nearest neighbor analysis in a GIS environment to associate the manholes with nodes in the computational mesh. If multiple manholes are assigned to the same node, we define the point source at that node based on the total outflow volumes from the manholes. In Safer_RAIN, the total runoff per manhole is added to the corresponding pixel in the computational mesh. On the other hand, in Hydro_AS-2D, the total runoff from the manholes is represented as a point source or nodal boundary condition. This means that the volume is distributed uniformly over the duration of 90 min.

4. Results

4.1. Rural Inundations from Minor Streams

4.1.1. Preliminary Sensitivity Analyses

In the case of rural inundations from minor streams, we had to perform a set of preliminary analyses first in order to identify the settings for HEC-RAS benchmarking simulations. Therefore, we develop multiple HEC-RAS models that we construct using the available 1 m resolution LiDAR DEM, and we implement a mesh that incorporates the buildings' footprints as break lines. In all rural areas within the models, we assign a Manning's coefficient of 0.033, as previously discussed [49]. To accurately simulate the embankment breaching phenomena, we apply different boundary conditions along the frontier of the computational mesh. Specifically, along the Pisciatello stream (Southern border), embankment breaches are added in the models. All simulated breaches are set to a width of 100 m, and no outflow is enabled due to the presence of the levee and hanging riverbed conditions. Additionally, a local energy slope of 1 perpendicular to each breach is incorporated in all HEC-RAS simulations. For the Northern and Eastern frontiers of the computational mesh, a free outflow boundary condition is set.

The Diffusion Wave equations are utilised in all simulations and detailed information on HEC-RAS simulations is described in Table 1. To ensure a balance between computation accuracy and runtime, we employ timesteps of 1 s or 15 s, depending on the specific case (refer to Table 2). In order to conduct a sensitivity analysis, we compare three groups of HEC-RAS simulations: (1) different resolutions for the computational grids (1 m or 5 m), (2) LiDAR DEMs with or without extruded buildings, and (3) various inflows represented by flow hydrographs a, b, and c in Figure 3a. These initial comparisons aim to determine the optimal trade-off between runtime and mesh resolution for HEC-RAS simulations, as well as to assess the impact of different input data and representations of the urban environment.

Table 1. HEC-RAS simulation information.

Simulation	Runtime	Error (m)	Relative Error	Outflow 1000 m³	Ending Vol 1000 m³
Breach 1 (HR_1)	12:19:13	0.1244	0.02	3.6	603.1
Breach 2 (HR_2)	13:11:16	0.1455	0.024	0	606.7
Breach 3 (HR_3)	13:05:23	0.1326	0.022	0	606.7
Breach 4 (HR_4)	12:31:00	0.1621	0.027	0	606.8
Breach 5 (HR_5)	6:24:37	0.1023	0.017	0	606.7
Breach 6 (HR_6)	4:16:51	0.07421	0.012	0	606.7
Breach 7 (HR_7)	4:01:02	0.05888	0.010	0	606.7

Table 2. Input data used in HEC-RAS simulations.

Simulation	Study Area Dimension (ha)	Computational Grid Size (m²)	Upstream Boundary Condition (Flow Hydrograph)	Downstream Boundary Condition (Normal Depth Friction Slope)		Computation Interval (s)
				BCL2	BCL3	
HR_TA1	50	1 × 1	a	0.003	0.0035	1
HR_TA5	50	5 × 5	a	0.003	0.0035	1
HR_TB1	50	1 × 1	a	0.003	0.0035	1
HR_Q67.4	1352	5 × 5	a	0.003	0.0005	15
HR_Q10	1352	5 × 5	b	0.003	0.0005	15
HR_Q5	1352	5 × 5	c	0.003	0.0005	15
HR_breach 1-7 (HR_7)	1352	5 × 5	a	0.003	0.0005	15

Effects of Mesh Resolution

The two simulations conducted over the test area utilise a 1 m resolution computational mesh generated from the LiDAR DEM with extruded buildings, which accounts for the complex morphology. In both cases, we adopt the flow hydrograph (a) to assess the impact of 1 m and 5 m resolutions on the modelling of inundation. The location of the simulated breach and the downstream outlet boundary condition lines (BCL2 and BCL3) are indicated in Figure 3. Energy slopes of 0.003 and 0.0035, obtained from the LiDAR DEM, are assigned to BCL2 and BCL3, respectively. To ensure numerically stable and accurate solutions, the computation interval for solving the Diffusion Wave equations is set to 1 s in both cases. Our results indicate very minimal differences between the output of the HR_TA1 and HR_TA5 simulations, as evidenced by the Flood Area Index (FAI) results presented in Table 3. The FAI values for both simulations, in terms of maximum water depth and end water depth, are nearly 1, indicating negligible differences between the two simulations. Therefore, for the remaining part of our study, we conduct HEC-RAS simulations with a 5 m resolution, which is computationally feasible, and compare them to Safer_RAIN simulations with a 1 m resolution.

Table 3. FAI values for comparisons of HECRAS and Safer_RAIN simulations.

Comparison	FAI Max Water Depth	FAI End Water Depth
HR_TA1 vs. HR_TA5 (Effect of different grid resolutions)	0.970	0.803
HR_TA1 vs. HR_TB1 (Effect of buildings)	0.946	0.980
HR_Q67.4 vs. HR_Q10 (Effect of inflow dynamics)	0.540	0.873
HR_Q67.4 vs. HR_Q5 (Effect of inflow dynamics)	0.431	0.698
SR_1 vs. HR_1 (Simulated with 1 breach)	0.147	0.318
SR_7 vs. HR_7 (Simulated with 7 breaches)	0.367	0.480
SR_all vs. HR_7 (Effects of breach locations)	0.372	0.480

Extruded Buildings vs. Building Resistance

The modelling of the inundation in the Test Area does not involve extruding the buildings at a 1 m grid resolution. Instead, a spatially variable Manning's roughness coefficient is adopted. In the literature [50], the "building resistance" method is employed to assess the sensitivity of Manning coefficients for flood inundation in idealized urban districts. To account for the resistance effect of buildings in the simulated area, a significantly high Manning coefficient value is assigned. The range of Manning coefficients tested in [50] varied from 10^0 to 10^{10} s·m$^{-1/3}$. Based on this information, we have chosen to utilise a Manning coefficient of 10 s·m$^{-1/3}$ over the building footprints in our study given the sparseness of buildings in the rural study area. In terms of the outlet boundary conditions and computational time interval used in this simulation (HR_TB1), they are the same as in simulation HR_TA1. Consequently, the extent of inundation and the simulated water depths in areas without buildings are very similar between simulations HR_TA1 and HR_TB1. Based on the FAI values presented in Table 3, it is noteworthy that both HR_TA1 and HR_TB1 are associated with values close to 1 in both the maximum and end scenarios. This indicates that they are capable of producing similar flooded areas. This finding carries particular significance in the context of sparsely populated rural areas, where building density is low. In such scenarios, it can be concluded that HR_TA1 and HR_TB1 can be used interchangeably, as they yield comparable results.

Impact of Different Inflow Hydrographs

The final set of comparisons in assessing the sensitivity of HECRAS simulations focuses on the inflow hydrographs. Specifically, we compare the HECRAS output associated with hydrograph (a), which is used for comparisons in the previous subsections, with the output resulting from inflow hydrographs (b) and (c). These hydrographs are associated with a slower breaching mechanism and are depicted in Figure 3a. To conduct these comparisons, we perform three additional simulations that cover the entire study area. These simulations are based on the results of the previously described tests and utilise a computational mesh with a resolution of 5 m and an increased roughness coefficient. Each simulation is named after the peak inflow of the corresponding hydrograph. Therefore, we have HR_Q67.4, HR_Q10, and HR_Q5 for hydrographs (a), (b), and (c), respectively. All three scenarios consider the same breach location, which is breach number 1 as indicated in Figure 3b. Additionally, the simulations adopt energy gradients of 0.003 and 0.0005 for the outflow boundary conditions BCL2 and BCL3, respectively, as shown in Figure 3b. For consistency, the time step for all simulations is set to 15 s.

When examining the pixel-based maximum simulated water depth, the results indicate that HR_Q67.4 is associated with the largest overall inundated area and the highest simulated water depths. Comparing the HEC-RAS output among the three simulations, it is evident that the distribution of maximum water depth is similar across all scenarios. Additionally, simulated maximum water depths exceeding 1 m are primarily concentrated in a limited portion of the study area, as depicted in Figure 6a. However, if we shift our focus to the distribution of simulated pixel-based water depths at the end of the simulation, the differences between the three scenarios become negligible, as shown in Figure 6b.

HEC-RAS Benchmarking Simulations

Based on the results of the aforementioned three preliminary sensitivity analyses, we decided to utilise a computational mesh with a resolution of 5 m spanning the entire study region. LiDAR DEM with extruded buildings clearly displays buildings' function in flooding and produces a more realistic inundation result, so LiDAR DEM with extruded buildings is used. Furthermore, all simulations consider inflow hydrograph (a), which is associated with a rapid breach formation and a 200-year flood volume. This decision is made as a conservative approach and illustrated in Figure 6. These settings are implemented to simulate seven inundation scenarios, each corresponding to a synthetic breach. The locations of these breaches, as well as the lines indicating the outlet boundary conditions,

can be seen in Figure 3b. The breaches are spaced approximately 1000 m apart. Table 2 provides an overview of the key details for each of the seven HEC-RAS runs, offering basic information on each scenario.
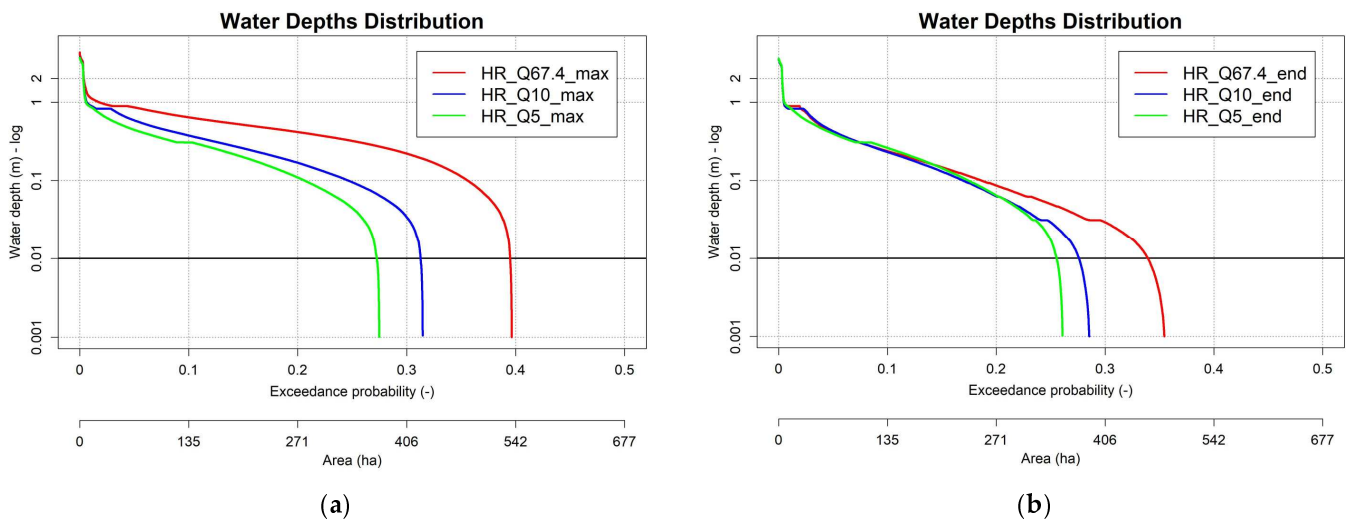
Figure 6. (**a**) Maximum water depth distribution between HR_Q67.4 and HR_Q10 simulations. (**b**) End water depth distribution between HR_Q67.4 and HR_Q5 simulations.

The results of the seven HEC-RAS simulations are combined to generate a unified inundation scenario known as HR_7 (HR_breach 1-7). This scenario encompasses the entire study region and represents the potential formation of breaches at any location along the Pisciatello stream. The HR_7 inundation scenario represents a flood event with a 200-year return period and includes two types of pixel-based simulated water depths. The first type consists of the local maximum water depth obtained at the end of the simulation (end). The second type comprises the local maximum water depth among all simulated maxima for the seven synthetic breaches (max). By incorporating both end and max water depths, HR_7 provides a comprehensive representation of the potential flood extents and depths across the study area. In addition to HR_7, our study also examines a single breach inundation scenario called HR_1. HR_1 is the HEC-RAS simulation conducted for breach 1, as illustrated in Figure 3b. This scenario utilises the same settings as described previously and includes the end and max simulated water depths. Both HR_1 and HR_7 serve as benchmark scenarios to evaluate the output of Safer_RAIN, allowing for comparison and assessment of its accuracy and reliability in simulating flood events.

4.1.2. Fluvial Flooding Simulation with Safer_RAIN and Comparison with Bench-Marking Scenarios

In this study, we use Safer_RAIN to generate inundation scenarios for the study area resulting from fluvial flooding, originating from the Pisciatello stream. Our focus is on the entire study area, and we accurately represent its morphology using the available 1 m resolution LiDAR DEM with extruded buildings. To identify areas prone to flooding, we pre-process the digital elevation model by identifying "blue spots" and their corresponding watersheds. In this case, we specifically consider blue spots larger than 300 m^2. We further analyse the morphological characteristics of these blue spots by employing a vertical discretization (slicing) of 0.05 m. One advantage of Safer_RAIN is that it simplifies the simulation process by only requiring the inflow flood volume as input. Unlike other methods, there is no need to select a specific hydrograph shape. Therefore, for each synthetic breach, generating the inundation scenario using Safer_RAIN simply involves inputting the overall inflow flood volume, which in this case is 606.600 m^3.

We examine three distinct Safer_RAIN scenarios, each focusing on pixel-based inundation water depth. The first scenario, SR_1, specifically considers the inundation that occurs

when the inflow flood volume is input at breach 1. The second scenario, SR_7, encompasses simulated water depths obtained from seven runs of Safer_RAIN, with each run receiving the flood volume at one of the seven breach locations. Lastly, the SR_all scenario utilises the input flood volume in all the blue-spot watersheds that share a frontier segment with the left Pisciatello embankment. While SR_7 and SR_all are similar inundation scenarios, SR_all is more conservative as it includes all the blue spots adjacent to the Pisciatello stream, whereas SR_7 may miss some due to the regular spacing of synthetic breaches. To evaluate these scenarios, we compare the output of SR_1 with the bench-marking end and maximum scenarios of HR_1, while SR_7 and SR_all are compared with scenarios of HR_7.

As anticipated, when comparing the Safer_RAIN scenarios SR_7 and SR_all, we observe very similar output with a slightly larger overall inundated area for SR_all. To assess the performance of Safer_RAIN in comparison to HEC-RAS inundation scenarios, which serve as a benchmark, we find that the end scenarios exhibit higher Flooded Area Index (FAI) values relative to the maximum scenarios. This outcome is expected due to the hydrostatic nature of Safer_RAIN flooding. When comparing FAI indices between Saf-er_RAIN and HEC-RAS scenarios, the comparisons with end water depth yield values around 0.5, while the comparisons with maximum water depth reduce to approximately 0.3. The maximum scenarios for HR_1 and HR_7 demonstrate larger overall inundated areas than their corresponding Safer_RAIN counterparts (i.e., SR_1, SR_7, and SR_all in this order). Figure 7 provides examples of raster maps utilised for computing FAI indices, highlighting areas where the two approaches align and areas where they differ. Additionally, a pixel-based comparison between simulated water depths reveals that Safer_RAIN values are either equal to or smaller than the corresponding values simulated by HEC-RAS (maximum scenarios). Some examples are shown in Figure 8 for further clarification.


(**a**)   (**b**)
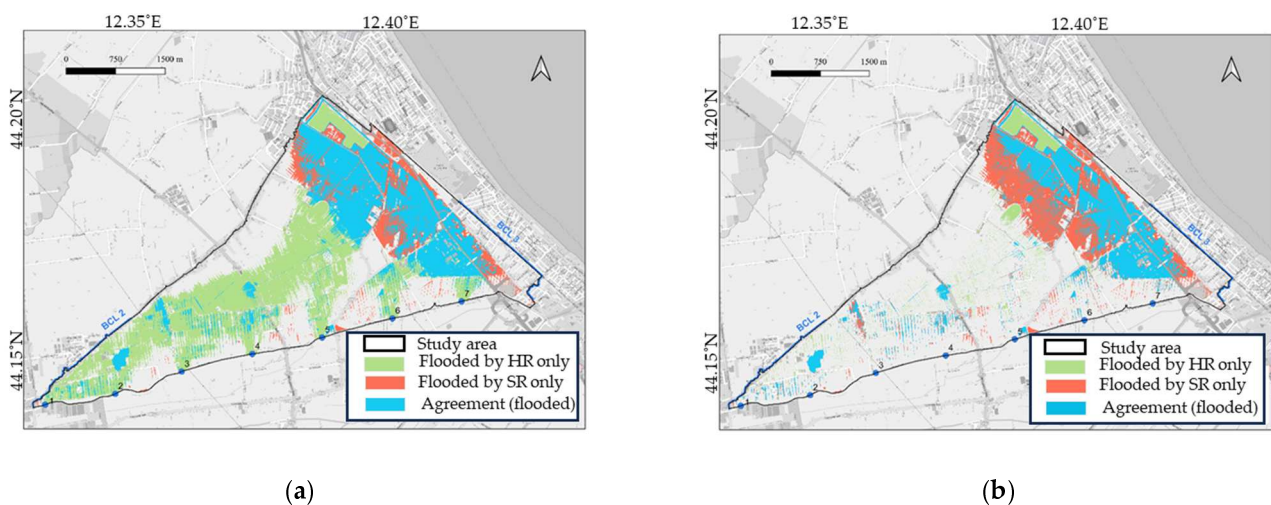
Figure 7. (**a**) Pixel-based comparison between inundated areas according to Safer_RAIN scenario SR_all and HEC-RAS inundation scenarios HR_7 max; (**b**) pixel-based comparison between inundated areas according to Safer_RAIN scenario SR_all and HEC-RAS inundation scenarios HR_7 end.

However, it is important to note that areas that are flooded only in HEC-RAS scenarios tend to have simulated water depths that are generally smaller than 1.0 m. Additionally, the majority of pixel-based differences between Safer_RAIN(SR) and HEC-RAS (HR) simulated water depths fall within the range of 0.1 m to 1.0 m. In terms of inundation ex-tent, Safer_RAIN and HEC-RAS scenarios, particularly the HR end scenarios, exhibit rather similar results (refer to Figures 7 and 8). It is worth mentioning that Safer_RAIN simulations tend to show larger inundations and accumulated flood volumes than HEC-RAS in the easternmost portion of the study area, which corresponds to the downstream section. Furthermore, more flood volume is accumulated at the bottom of the study area in the Safer_RAIN simulations. Finally, in Figure 9, a representation of water depth distribu-

tions and water depth differences between Safer_RAIN and HEC-RAS simulations for all breaches is reported.
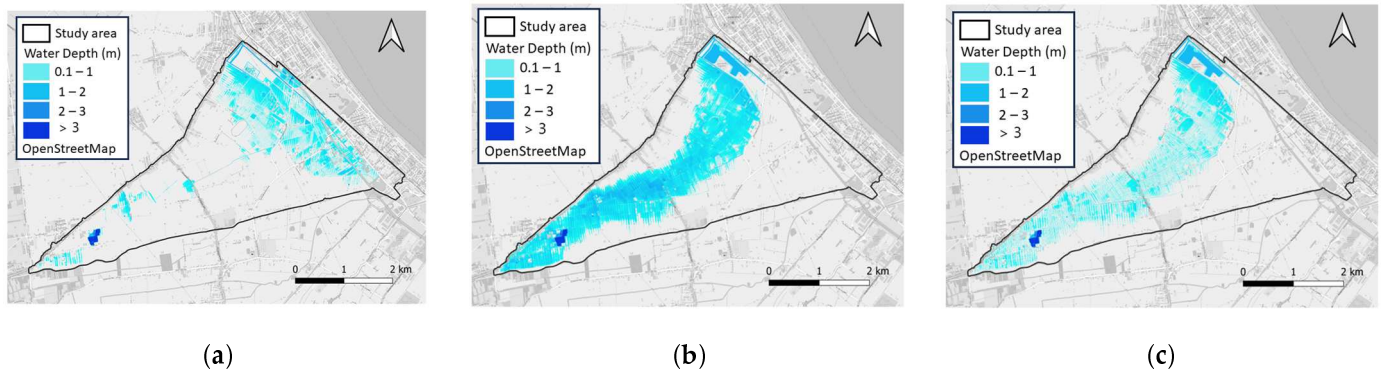
Figure 8. (**a**) Safer_RAIN simulated water depth at breach 1 (SR_1); (**b**) HEC-RAS maximum simulated water depth at breach 1 (HR_1, max); (**c**) HEC-RAS final simulated water depth at breach 1 (HR_1, end).
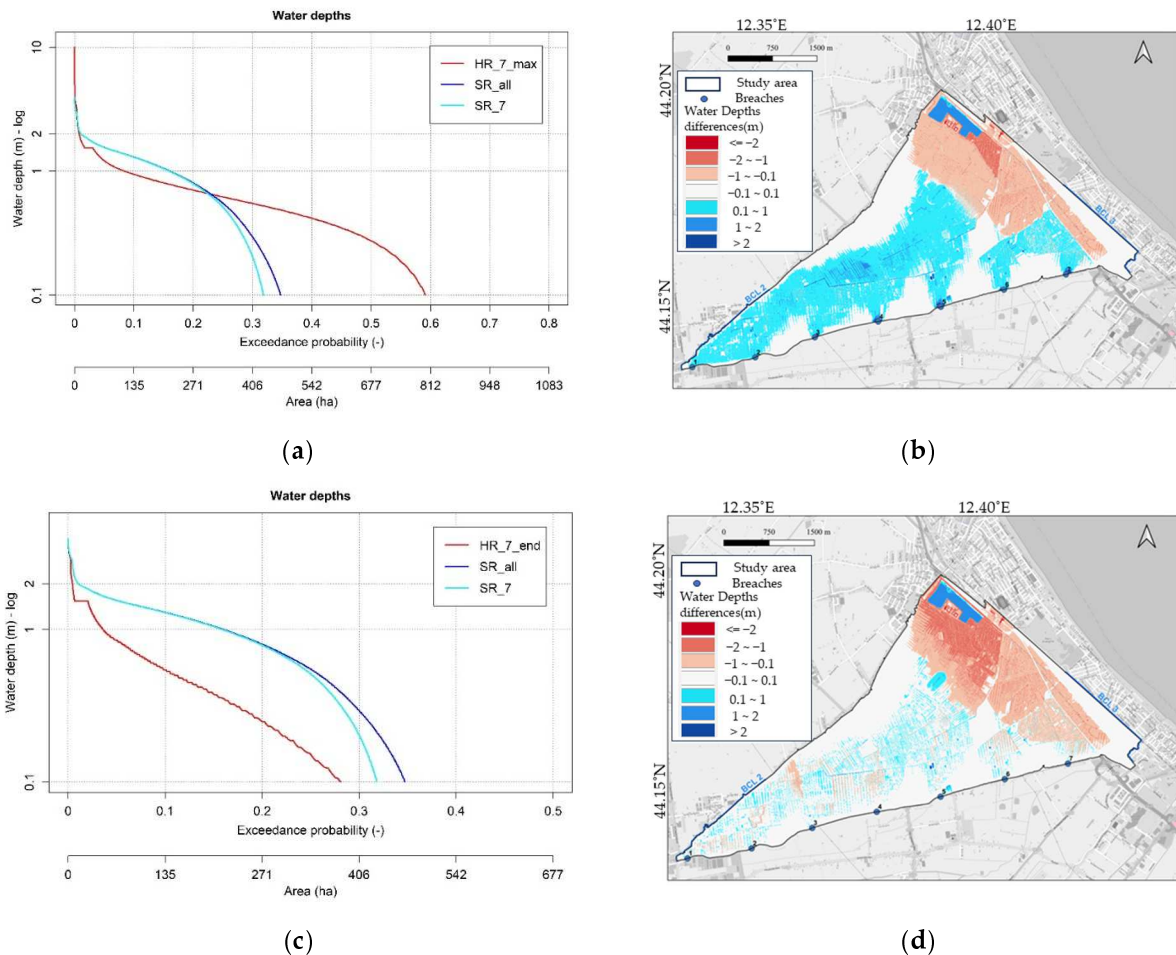

Figure 9. (**a**) Simulated water depth distributions between HR_7_max, SR_all and SR_7. (**b**) Water depth differences between SR_all and HR_7_max. (**c**) Simulated water depth distributions between HR_7_end, SR_all and SR_7. (**d**) Water depth differences between SR_all and HR_7_end.

4.2. Urban Inundations from Drainage System Outflows

To address urban inundations caused by drainage system outflows, our study focuses on evaluating the concurrence between two modelling methodologies. We achieve this by

comparing the simulated water depth distributions from both models and analysing the corresponding differences in water depth across the computational domain. We evaluate the concurrence between the two modelling methodologies by comparing simulated water depth distributions from both models and analysing the corresponding differences in water depth across the computational domain. We illustrate these comparisons using scatterplots and maps. For each scenario (20, 50, 100-year return period), we consider two distinct outputs from Hydro_AS-2D: the local maximum value of simulated water depth (max. scenario), which represents the highest recorded water depth regardless of the time step, and the simulated water depths at the end of the 5 h simulation (end scenario) to ensure that the entire outflow volume has reached its final destination. Both models do not account for infiltration, resulting in conservative inundation scenarios. Figure 4c illustrates the differences in water depths obtained by Hydro_AS-2D after a 5 h simulation and computed by Safer_RAIN. In this illustration, red areas indicate an overestimation of Safer_RAIN, while blue areas indicate where water depths simulated by Safer_RAIN are lower than those simulated by Hydro_AS-2D.

The scatterplot density diagram in Figure 10a compares the water depths simulated with Safer_RAIN to the corresponding water depths obtained from Hydro_AS-2D for both the max and end inundation scenarios. The diagrams use a logarithmic scale to provide better visualization of the entire range of simulated data, which spans across two orders of magnitude. The bisecting line, also known as the 1:1 line, in the first quadrant, represents the line of perfect fit. As observed in the scatterplot density diagrams, the points are distributed around the 1:1 line. However, there is a significant scatter around the line itself, indicating only a fair agreement between the two models. It is worth noting that the agreement is noticeably better when considering the end scenario, which represents the water depths after 5 h from the start of the event.

(a)   (b)   (c)
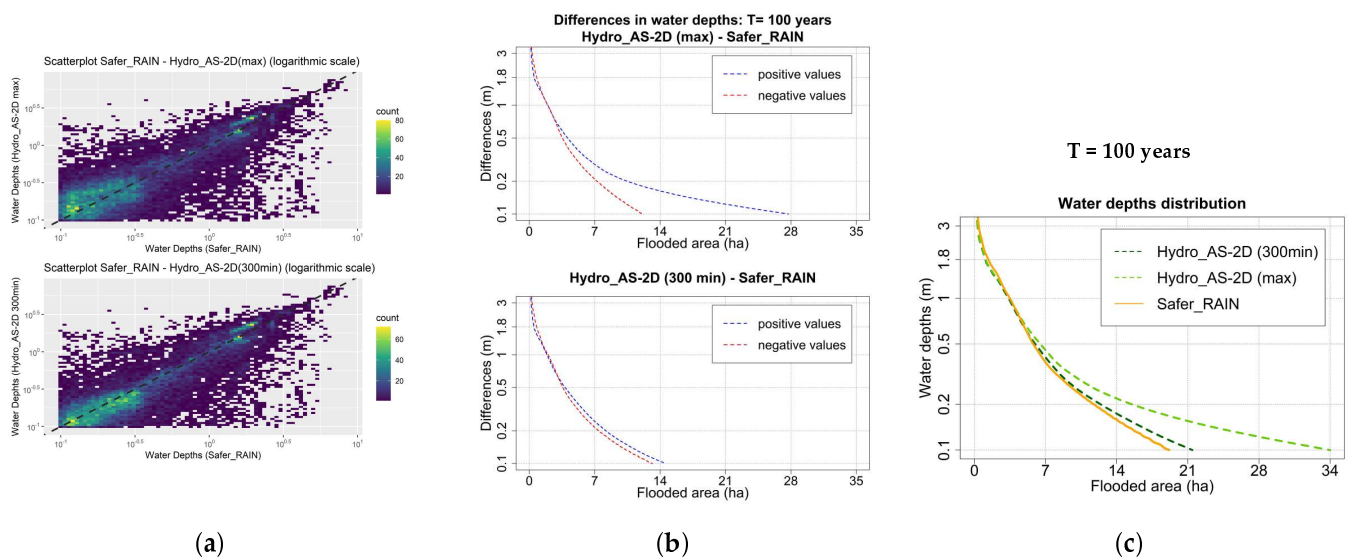
Figure 10. (**a**) Comparison between pixel-based water depths simulated by Safer_RAIN and HYDRO_AS-2D for max and end (300 min) scenarios; (**b**) non-exceedance probability of simulated water depth (positive and negative) differences in 100-year return period under max and end (300 min) scenarios; (**c**) water depth distribution between water depth and flooded area in terms of Hydro_AS-2D (300 min and max) and Safer_RAIN simulations.

Figure 10b,c depict the distribution of simulated water depth and differences in simulated water depth across the study area. These differences are calculated on a pixel-by-pixel basis, distinguishing between positive and negative variances. Each graph represents the area (in hectares) where simulated water depths or their differences are greater than or equal to a certain value. Figure 10c contrasts the simulated inundation water depths for a 100-year event produced by Safer_RAIN and Hydro_AS-2D five hours into the inundation

event, as well as the maximum values generated by the hydrodynamic model. Focusing on water depths over 20 cm, a common threshold of uncertainty in hydrodynamic simulations, the distributions of simulated water depths are strikingly alike, including the overall extent of inundation. The output from Safer_RAIN is nearly identical to Hydro_AS-2D in terms of water depth distribution. This similarity extends to the distribution of differences in simulated water depths. However, Figure 10b,c reveal that despite the overall similarity of simulated water depth distribution between the two models, there can be considerable local variations. It is also important to note that differences greater than 1 m are quite rare across the study area. The results obtained for a return period of 20 years are very similar and are not reported here for the sake of conciseness.

5. Discussion

5.1. Rural Inundations from Minor Streams

The differences between the inundation scenarios generated from the two algorithms, Safer_RAIN and HEC-RAS, are expected to give the different nature of the two approaches: hydrostatic for the former, and hydrodynamic for the latter. Safer_RAIN cannot simulate back-water effects and hydrodynamic routing [26]. Based on the analysis of FAI values in the comparison of Safer_RAIN and HEC-RAS simulations, it is evident that the end water depth scenarios consistently exhibit higher FAI values when compared to the maximum water depth scenarios. This suggests that the extent of flooding is greater in the end scenarios as predicted by both models. Furthermore, the level of flooded area agreement between Safer_RAIN and HEC-RAS varies depending on the water depth scenario. In the end water depth scenarios, there is a satisfactory level of agreement between the two approaches. However, in the maximum water depth scenarios, the agreement is weaker, suggesting some discrepancies between the models. In terms of water depth and inundation area results, it is important to note that Safer_RAIN, being a hydrostatic model, tends to underestimate water depth when compared to the hydrodynamic model HEC-RAS. Additionally, the overall inundated areas tend to be underpredicted by Safer_RAIN. This limitation is inherent in the hydrostatic nature of Safer_RAIN [26] and we are currently working on empirical strategies to address and reduce this constraint. However, the agreement between Safer_RAIN and HEC-RAS end inundation scenarios is encouraging and indicates that the current version of the simplified inundation algorithm is already capable of providing useful information for rural flood risk mitigation and civil protection activities (e.g., rural land management to the alleviation of flood risk) [51]. Also, the flatter the area, the more accurate and reliable Safer_RAIN simulated water depths are.

There is an unexpectedly larger inundation simulated by Safer_RAIN in the downstream portion of the study area compared to HECRAS in the end water depth scenario (see Figure 9). This can be attributed to two factors. Firstly, the hydrodynamic nature of HEC-RAS simulations results in the production of outflowing water volumes through the outlet boundary condition line BCL2 (as depicted in Figure 9b). In contrast, Safer_RAIN, being hydrostatic in nature, does not generate such outflow volumes (as indicated in Table 1, where HEC-RAS simulation for breach 1 produces outflow volumes). As a result, this water will not propagate towards the downstream section of the study area in Safer_RAIN simulations. Secondly, Safer_RAIN does not inundate dike areas that may be flooded by a hydrodynamic numerical scheme like the one employed by HEC-RAS [52]. This is particularly relevant when the height of the embankment is limited. An example can be observed in the upper corner of the study area, where HEC-RAS only simulates a large "F" shaped area of flooding. However, these water volumes will not reach the downstream portion of the study area in HEC-RAS simulations. Nevertheless, it is worth noting that Safer_RAIN has the capability to simulate the potential flooded area resulting from breaches, providing valuable information that is essential for rural communities [29]. This information helps them understand and effectively address the challenges associated with flooding incidents.

It is important to highlight that HEC-RAS hydrodynamic simulations come with high computational costs, which forced us to significantly reduce the mesh resolution. For

instance, a single simulation at a resolution of 5 m (or 1 m) can take more than 6 h (or half a day) to complete. This factor emphasizes the computational efficiency and simplicity of Safer_RAIN in comparison. In this study, all simulations are conducted on a computer with 64 bytes, a 3.4 GHz CPU, 8 MB cache, and 16 GB RAM. The HEC-RAS simulations took a maximum of 13 h and a minimum of 4 h to obtain results with a 5 m resolution. If the HEC-RAS simulations are conducted with a 1 m resolution, it would take weeks to complete the computation. On the other hand, all Safer_RAIN simulations, encompassing various scenarios, are completed within half a day. This clearly demonstrates the efficiency and simplicity of Safer_RAIN in computational terms. Therefore, Safer_RAIN can be utilised for near real-time flood detection in rural areas by leveraging the combined use of high-resolution remote sensing data [53].

5.2. Urban Inundations from Drainage System Outflows

In the context of our application in urban inundations, there are some restrictions concerning the data integration of the hydrodynamic model from MM Spa. This model is privately owned, so the underlying data and details of the model structure are not freely accessible. The proposed integration between Safer_RAIN and the MM Spa model consists of a model cascade rather than a model coupling, the output of the MM Spa model is fed into Safer_RAIN. This means that feedback and interactions between different hydrologic components of the two models are not accounted for (see e.g., [54]). Although this schematization is suitable for a preliminary analysis like the one we present here, we acknowledge that future studies and research are needed to address the impact of this simplification and to investigate viable solutions. Although a local comparison of simulation results from Safer_RAIN and Hydro_AS-2D reveals some significant differences in simulated water depths, the overall representations of inundation, including inundation extent and water depth distributions, are in good agreement between the two models.

Hydro_AS-2D is a hydrodynamic model that operates fully in two dimensions, whereas Safer_RAIN is an algorithm that uses DEM to simulate the filling and overflowing of water, using the mass balance equation for modelling [26]. The urban drainage network system is widely recognized as a major contributor to urban inundations [33,34]. Numerous studies have indicated that inadequate planning or insufficient capacity of the drainage system can lead to urban flooding, primarily due to excessive discharge volumes [35–37]. To address this issue, our study focuses on demonstrating the effectiveness of Safer_RAIN in simulating urban flooding caused by water volume overflow from manholes during drainage network surcharges. This simulation proves valuable, particularly when a reliable numerical model of the drainage network is available. By utilising Safer_RAIN, we aim to bridge the existing gap and provide insights into managing and mitigating urban flooding risks effectively.

It is worth noting here that also, in this case, hydrodynamic modelling proved to be highly intensive; Hydro_AS-2D requires 5 h to simulate the entire study area, which is equivalent to 40 min on a high-performance computer with an Intel Xeon W-2400 CPU. Safer_RAIN completes the Flooding Phase in just 20 s on the same hardware. Furthermore, the analysis of drainage system outflows using our application, Safer_RAIN, has revealed its exceptional capabilities in terms of fast processing and computation [45]. This means that Safer_RAIN can perform calculations and predictions in real time, even at high resolutions, making it highly suitable for nowcasting applications [55]. This feature provides a significant advantage in civil protection activities and emergency management. In critical situations such as severe weather events or natural disasters, having access to up-to-date and accurate information is crucial for making informed decisions and taking prompt action to ensure the safety and well-being of affected communities. With Safer_RAIN's fast processing and computation, civil protection agencies and emergency management teams can effectively monitor and analyse drainage system outflows in real time.

6. Conclusions

Our study focuses on Safer_RAIN, a fast-processing inundation algorithm available on the SaferPlaces web-based platform (see https://saferplaces.co/ (accessed on 15 Janunary 2024)) [26]. Safer_RAIN, originally designed for high-spatial-resolution simplified modelling and mapping of flood hazards in urban areas affected by severe rainstorms, is used in our study to simulate inundation and flooding scenarios resulting from point-source water volumes with two different origins: (a) flooding from small stream breaching levee systems in rural and predominantly flat peri-urban areas, and (b) stormwater volumes overflowing from urban drainage systems during extremely severe rainfall events that exceed the drainage system's capacity.

Concerning application (a), we focus on simulating levee breaching and floodplain inundation in one of the floodplains of the Pisciatello stream in Northern Italy. We use a fully 2D hydrodynamic model (HEC-RAS) and Safer_RAIN for this simulation. In application (b), we focus on a district in the city of Milan, Italy, which is prone to pluvial flooding. We compare the inundation simulated by Safer_RAIN with the output from a fully 2D hydrodynamic model. Although there are differences between the results of Safer_RAIN and the two hydrodynamic models, which are expected due to the different approaches (hydrostatic for Safer_RAIN vs. hydro-dynamic for the benchmarking models), our application shows that Safer_RAIN is a valuable and effective tool for mapping rural and urban inundation caused by point-source volumes at a high horizontal resolution of approximately 1 m.

In conclusion, our application and tests demonstrate the versatility and flexibility of the Safer_RAIN module, even when used in contexts beyond its intended application domain (i.e., mapping inundation caused by severe rainstorms), proving to be useful for modelling the effects of insufficiencies in rural small stream levee systems or urban drainage systems. Safer_RAIN performs exceptionally well in predominantly flat terrain, making it particularly effective in scenarios where immediate response after a flooding event is crucial, such as managing evacuation logistics and rescue operations.

Author Contributions: Conceptualization, K.K.K., F.B., H.W., S.B., P.M., P.P.A., S.P. and A.C.; methodology, S.B., A.C. and S.P., software, S.B. and P.M.; formal analysis, K.K.K., F.B. and H.W., investigation, K.K.K., F.B. and H.W., writing—original draft preparation, K.K.K. and F.B.; writing—review and editing, K.K.K., S.B., P.M. and A.C.; visualization, K.K.K., F.B. and H.W.; supervision, S.B., P.M. and A.C.; project administration, S.B., P.M. and A.C.; funding acquisition, S.B., P.M. and A.C. All authors have read and agreed to the published version of the manuscript.

Institutional Review Board Statement: Not applicable.

Informed Consent Statement: Not applicable.

Data Availability Statement: LiDAR data for Digital Elevation Models, and OpenStreetMap data for Building footprints used in this study are openly accessible. The outflow volumes from manholes during major storms are obtained from Metropolitana Milanese Spa (MM Spa), however they are not publicly accessible as they are the property of MM Spa.

Conflicts of Interest: The authors declare no conflicts of interest.

References

1. Directorate-General for Environment (European Commission). *Strengthening the Synergies between Agriculture and Flood Risk Management in the European Union*; EU Publications: Brussels, Belgium, 2021. [CrossRef]
2. Colacicco, R.; Refice, A.; Nutricato, R.; D'addabbo, A.; Nitti, D.O.; Capolongo, D. High Spatial and Temporal Resolution Flood Monitoring through Integration of Multisensor Remotely Sensed Data and Google Earth Engine Processing. *EGU Gen. Assem.* **2022**, *1*. [CrossRef]
3. Kong, F.; Ban, Y.; Yin, H.; James, P.; Dronova, I. Modeling Stormwater Management at the City District Level in Response to Changes in Land Use and Low Impact Development. *Environ. Model. Softw.* **2017**, *95*, 132–142. [CrossRef]
4. Mishra, P.; Singh, D.; Yamaguchi, Y.; Singh, D. Land Cover Classification of Palsar Images by Knowledge Based Decision Tree Classifier and Supervised Classifiers Based on SAR Observables. *Prog. Electromagn. Res. B* **2011**, *30*, 47–70. [CrossRef]
5. European Commission. EU Flood Directive. *Off. J. Eur. Union* **2007**, *1*, 186–193. Available online: http://data.europa.eu/eli/dir/2007/60/oj (accessed on 15 January 2024).
6. Tsubaki, R.; Fujita, I. Unstructured Grid Generation Using LiDAR Data for Urban Flood Inundation Modelling. *Hydrol. Process.* **2010**, *24*, 1404–1420. [CrossRef]
7. Meesuk, V.; Vojinovic, Z.; Mynett, A.E.; Abdullah, A.F. Urban Flood Modelling Combining Top-View LiDAR Data with Ground-View SfM Observations. *Adv. Water Resour.* **2015**, *75*, 105–117. [CrossRef]
8. Tyrna, B.; Assmann, A.; Fritsch, K.; Johann, G. Large-Scale High-Resolution Pluvial Flood Hazard Mapping Using the Raster-Based Hydrodynamic Two-Dimensional Model FloodAreaHPC. *J. Flood Risk Manag.* **2018**, *11*, S1024–S1037. [CrossRef]
9. Saksena, S.; Merwade, V. Incorporating the Effect of DEM Resolution and Accuracy for Improved Flood Inundation Mapping. *J. Hydrol.* **2015**, *530*, 180–194. [CrossRef]
10. Fewtrell, T.J.; Duncan, A.; Sampson, C.C.; Neal, J.C.; Bates, P.D. Benchmarking Urban Flood Models of Varying Complexity and Scale Using High Resolution Terrestrial LiDAR Data. *Phys. Chem. Earth Parts A/B/C* **2011**, *36*, 281–291. [CrossRef]
11. Leitão, J.P.; Boonya-aroonnet, S.; Prodanović, D.; Maksimović, Č. The Influence of Digital Elevation Model Resolution on Overland Flow Networks for Modelling Urban Pluvial Flooding. *Water Sci. Technol.* **2009**, *60*, 3137–3149. [CrossRef] [PubMed]
12. Ernst, J.; Dewals, B.J.; Detrembleur, S.; Archambeau, P.; Erpicum, S.; Pirotton, M. Micro-Scale Flood Risk Analysis Based on Detailed 2D Hydraulic Modelling and High Resolution Geographic Data. *Nat. Hazards* **2010**, *55*, 181–209. [CrossRef]
13. Yin, J.; Yu, D.; Yin, Z.; Liu, M.; He, Q. Evaluating the Impact and Risk of Pluvial Flash Flood on Intra-Urban Road Network: A Case Study in the City Center of Shanghai, China. *J. Hydrol.* **2016**, *537*, 138–145. [CrossRef]
14. Patro, S.; Chatterjee, C.; Mohanty, S.; Singh, R.; Raghuwanshi, N.S. Flood Inundation Modeling Using MIKE FLOOD and Remote Sensing Data. *J. Indian Soc. Remote Sens.* **2009**, *37*, 107–118. [CrossRef]
15. Nguyen, P.; Thorstensen, A.; Sorooshian, S.; Hsu, K.; AghaKouchak, A. Flood Forecasting and Inundation Mapping Using HiResFlood-UCI and Near-Real-Time Satellite Precipitation Data: The 2008 Iowa Flood. *J. Hydrometeorol.* **2015**, *16*, 1171–1183. [CrossRef]
16. Wright, N.G.; Villanueva, I.; Bates, P.D.; Mason, D.C.; Wilson, M.D.; Pender, G.; Neelz, S. Case Study of the Use of Remotely Sensed Data for Modeling Flood Inundation on the River Severn, U.K. *J. Hydraul. Eng.* **2008**, *134*, 533–540. [CrossRef]
17. Jafarzadegan, K.; Merwade, V. A DEM-Based Approach for Large-Scale Floodplain Mapping in Ungauged Watersheds. *J. Hydrol.* **2017**, *550*, 650–662. [CrossRef]
18. Teng, J.; Vaze, J.; Dutta, D.; Marvanek, S. Rapid Inundation Modelling in Large Floodplains Using LiDAR DEM. *Water Resour. Manag.* **2015**, *29*, 2619–2636. [CrossRef]
19. Grimaldi, S.; Petroselli, A.; Arcangeletti, E.; Nardi, F. Flood Mapping in Ungauged Basins Using Fully Continuous Hydrologic–Hydraulic Modeling. *J. Hydrol.* **2013**, *487*, 39–47. [CrossRef]
20. Nardi, F.; Vivoni, E.R.; Grimaldi, S. Investigating a Floodplain Scaling Relation Using a Hydrogeomorphic Delineation Method. *Water Resour. Res.* **2006**, *42*. [CrossRef]
21. Manfreda, S.; Nardi, F.; Samela, C.; Grimaldi, S.; Taramasso, A.C.; Roth, G.; Sole, A. Investigation on the Use of Geomorphic Approaches for the Delineation of Flood Prone Areas. *J. Hydrol.* **2014**, *517*, 863–876. [CrossRef]
22. Manfreda, S.; Samela, C.; Gioia, A.; Consoli, G.G.; Iacobellis, V.; Giuzio, L.; Cantisani, A.; Sole, A. Flood-Prone Areas Assessment Using Linear Binary Classifiers Based on Flood Maps Obtained from 1D and 2D Hydraulic Models. *Nat. Hazards* **2015**, *79*, 735–754. [CrossRef]
23. Manfreda, S.; Di Leo, M.; Sole, A. Detection of Flood-Prone Areas Using Digital Elevation Models. *J. Hydrol. Eng.* **2011**, *16*, 781–790. [CrossRef]
24. Samela, C.; Manfreda, S.; De Paola, F.; Giugni, M.; Sole, A.; Fiorentino, M. DEM-Based Approaches for the Delineation of Flood-Prone Areas in an Ungauged Basin in Africa. *J. Hydrol. Eng.* **2016**, *21*, 06015010. [CrossRef]
25. Samela, C.; Troy, T.J.; Manfreda, S. Geomorphic Classifiers for Flood-Prone Areas Delineation for Data-Scarce Environments. *Adv. Water Resour.* **2017**, *102*, 13–28. [CrossRef]
26. Samela, C.; Persiano, S.; Bagli, S.; Luzzi, V.; Mazzoli, P.; Humer, G.; Reithofer, A.; Essenfelder, A.; Amadio, M.; Mysiak, J.; et al. Safer_RAIN: A DEM-Based Hierarchical Filling-&-Spilling Algorithm for Pluvial Flood Hazard Assessment and Mapping across Large Urban Areas. *Water* **2020**, *12*, 1514. [CrossRef]

27. Serra-Llobet, A.; Jähnig, S.C.; Geist, J.; Kondolf, G.M.; Damm, C.; Scholz, M.; Lund, J.; Opperman, J.J.; Yarnell, S.M.; Pawley, A.; et al. Restoring Rivers and Floodplains for Habitat and Flood Risk Reduction: Experiences in Multi-Benefit Floodplain Management From California and Germany. *Front. Environ. Sci.* **2022**, *9*, 778568. [CrossRef]

28. Auerswald, K.; Moyle, P.; Seibert, S.P.; Geist, J. HESS Opinions: Socio-Economic and Ecological Trade-Offs of Flood Management— Benefits of a Transdisciplinary Approach. *Hydrol. Earth Syst. Sci.* **2019**, *23*, 1035–1044. [CrossRef]

29. Krasiewicz, D.W.; Wierzbicki, G. Flood Perception from Local Perspective of Rural Community vs. Geomor-phological Control of Fluvial Processes in Large Alluvial Valley (the Middle Vistula River, Poland). *Hydrology* **2023**, *10*, 191. [CrossRef]

30. Zhu, Z.; Chen, Z.; Chen, X.; He, P. Approach for Evaluating Inundation Risks in Urban Drainage Systems. *Sci. Total Environ.* **2016**, *553*, 1–12. [CrossRef]

31. Skougaard Kaspersen, P.; Høegh Ravn, N.; Arnbjerg-Nielsen, K.; Madsen, H.; Drews, M. Comparison of the Impacts of Urban Development and Climate Change on Exposing European Cities to Pluvial Flooding. *Hydrol. Earth Syst. Sci.* **2017**, *21*, 4131–4147. [CrossRef]

32. Yazdanfar, Z.; Sharma, A. Urban Drainage System Planning and Design—Challenges with Climate Change and Urbanization: A Review. *Water Sci. Technol.* **2015**, *72*, 165–179. [CrossRef] [PubMed]

33. Astaraie-Imani, M.; Kapelan, Z.; Fu, G.; Butler, D. Assessing the Combined Effects of Urbanisation and Climate Change on the River Water Quality in an Integrated Urban Wastewater System in the UK. *J. Environ. Manag.* **2012**, *112*, 1–9. [CrossRef] [PubMed]

34. Makropoulos, C.K.; Butler, D. Distributed Water Infrastructure for Sustainable Communities. *Water Resour. Manag.* **2010**, *24*, 2795–2816. [CrossRef]

35. Zou, Q.; Zhou, J.; Zhou, C.; Guo, J.; Deng, W.; Yang, M.; Liao, L. Fuzzy Risk Analysis of Flood Disasters Based on Diffused-Interior-Outer-Set Model. *Expert Syst. Appl.* **2012**, *39*, 6213–6220. [CrossRef]

36. Peng, H.-Q.; Liu, Y.; Wang, H.-W.; Ma, L.-M. Assessment of the Service Performance of Drainage System and Transformation of Pipeline Network Based on Urban Combined Sewer System Model. *Environ. Sci. Pollut. Res.* **2015**, *22*, 15712–15721. [CrossRef] [PubMed]

37. Arora, A.S.; Reddy, A.S. Conceptualizing a Decentralized Stormwater Treatment System for an Urbanized City with Improper Stormwater Drainage Facilities. *Int. J. Environ. Sci. Technol.* **2015**, *12*, 2891–2900. [CrossRef]

38. Shustikova, I.; Domeneghetti, A.; Neal, J.C.; Bates, P.; Castellarin, A. Comparing 2D Capabilities of HEC-RAS and LISFLOOD-FP on Complex Topography. *Hydrol. Sci. J.* **2019**, *64*, 1769–1782. [CrossRef]

39. Schwarz, B. LIDAR Mapping the World in 3D. *Nat. Photonics* **2010**, *4*, 429–430. [CrossRef]

40. Balstrøm, T.; Crawford, D. Arc-Malstrøm: A 1D Hydrologic Screening Method for Stormwater Assessments Based on Geometric Networks. *Comput. Geosci.* **2018**, *116*, 64–73. [CrossRef]

41. Wu, Q.; Lane, C.R.; Wang, L.; Vanderhoof, M.K.; Christensen, J.R.; Liu, H. Efficient Delineation of Nested Depression Hierarchy in Digital Elevation Models for Hydrological Analysis Using Level-Set Method. *J. Am. Water Resour. Assoc.* **2019**, *55*, 354–368. [CrossRef]

42. Zhang, S.; Pan, B. An Urban Storm-Inundation Simulation Method Based on GIS. *J. Hydrol.* **2014**, *517*, 260–268. [CrossRef]

43. O'Callaghan, J.F.; Mark, D.M. The Extraction of Drainage Networks from Digital Elevation Data. *Comput. Vis. Graph. Image Process.* **1984**, *28*, 323–344. [CrossRef]

44. Green, W.H.; Ampt, G.A. The Flow of Air and Water through Soils. *J. Agric. Sci* **1911**, *4*, 1–24.

45. Mediero, L.; Soriano, E.; Oria, P.; Bagli, S.; Castellarin, A.; Garrote, L.; Mazzoli, P.; Mysiak, J.; Pasetti, S.; Persiano, S.; et al. Pluvial Flooding: High-Resolution Stochastic Hazard Mapping in Urban Areas by Using Fast-Processing DEM-Based Algorithms. *J. Hydrol.* **2022**, *608*, 127649. [CrossRef]

46. Brunner, G.W. HEC-RAS River Analysis System: Hydraulic Reference Manual, Version 5.0. *US Army Corps Eng. Eng. Cent.* **2016**, *547*.

47. Papaioannou, G.; Efstratiadis, A.; Vasiliades, L.; Loukas, A.; Papalexiou, S.M.; Koukouvinos, A.; Tsoukalas, I.; Kossieris, P. An Operational Method for Flood Directive Implementation in Ungauged Urban Areas. *Hydrology* **2018**, *5*, 24. [CrossRef]

48. Autorità dei Bacini Regionali Romagnoli. *Piano Stralcio per il Rischio*; Autorità dei Bacini Regionali Romagnoli: Regione Emilia Romagna, Italy, 2017; p. 181. Available online: https://www.adbpo.it/PAI/PAI_Bacini_Romagnoli/Variante_PAI_PGRA/Normativa_TestoCoord2017.pdf (accessed on 15 January 2024).

49. Chow, V.T. *Open Channel Hydraulics*; MacGraw Hill Kogakusha, Ltd.: Tokyo, Japan, 1959.

50. Li, Z.; Liu, J.; Mei, C.; Shao, W.; Wang, H.; Yan, D. Comparative Analysis of Building Representations in TELEMAC-2D for Flood Inundation in Idealized Urban Districts. *Water* **2019**, *11*, 1840. [CrossRef]

51. Morris, J.; Beedell, J.; Hess, T.M. Mobilising Flood Risk Management Services from Rural Land: Principles and Practice. *J. Flood Risk Manag.* **2016**, *9*, 50–68. [CrossRef]

52. Carisi, F.; Domeneghetti, A.; Gaeta, M.G.; Castellarin, A. Is Anthropogenic Land Subsidence a Possible Driver of Riverine Flood-Hazard Dynamics? A Case Study in Ravenna, Italy. *Hydrol. Sci. J.* **2017**, *62*, 2440–2455. [CrossRef]

53. Mason, D.C.; Davenport, I.J.; Neal, J.C.; Schumann, G.J.-P.; Bates, P.D. Near Real-Time Flood Detection in Urban and Rural Areas Using High-Resolution Synthetic Aperture Radar Images. *IEEE Trans. Geosci. Remote Sens.* **2012**, *50*, 3041–3052. [CrossRef]

54. Martínez, C.; Vojinovic, Z.; Price, R.; Sanchez, A. Modelling Infiltration Process, Overland Flow and Sewer System Interactions for Urban Flood Mitigation. *Water* **2021**, *13*, 2028. [CrossRef]
55. Zanchetta, A.D.L.; Coulibaly, P. Recent Advances in Real-Time Pluvial Flash Flood Forecasting. *Water* **2020**, *12*, 570. [CrossRef]